# Filament-free 4D Printing of Shape Memory Polymer Foams: Towards Multifunctional Adaptive Foam-Based Structures

R. Dagur[1], M. Nofar[2], and C. Ayranci[1*]

[1] Department of Mechanical Engineering, University of Alberta, Edmonton, Alberta, T6E 3A3, Canada, [2] Metallurgical & Materials Engineering Department, Faculty of Chemical and Metallurgical Engineering, Istanbul Technical University, Maslak, Istanbul 34469, Turkey

* *Corresponding author (cayranci@ualberta.ca)*

**Keywords:** *Shape-memory polymer; foaming, 4D printing; chemical blowing agent; pellet-based printing; filament free printing*

## 1. Abstract

Cellular thermoplastic foams are essential engineering materials for lightweight design, energy absorption, thermal insulation, and control of functional properties. Consequently, the 3D printing of foams using extrusion-based additive manufacturing (EBAM) processes, also known as FDM or FFF is an emerging field in recent years. However, comparatively very little work has addressed the 4D printing of foams by EBAM. In this study, we report our initial findings on filament-free 4D printing of shape-memory polyurethane (SMPU) foams produced with chemical blowing agent (CBA) Azodicarbonamide using our custom-built pellet-based EBAM system. We discuss our findings on the effects of printing processing on density reduction, cellular morphology and thermally activated shape-memory responses. The results show that pellet-based in situ foaming can produce lightweight SMPU foams while preserving shape-memory functionality, but also demonstrate that foaming, morphology, and recovery are strongly related. This study provides a foundation and will open avenues towards producing multifunctional, adaptive, foam-based lightweight structures that are difficult to achieve with conventional manufacturing or filament-based printing. This is an appealing approach for creating complex actuating geometries for applications in soft robotics, deployable aerospace structures, and morphing systems.

## 2. Introduction

Cellular thermoplastic foams have become important engineering materials because they provide low weight, energy absorption, thermal insulation, and property control through internal porosity [1,2]. These features make them useful in transportation, packaging, protective structures, insulation, biomedical devices, and lightweight components where stiffness, damping, thermal management, and energy absorption must be balanced with reduced density. Traditionally, polymer foams are produced by molding, extrusion, or post-foaming routes, in which the final geometry and cellular structure are often controlled in a separate process. Extrusion-based additive manufacturing (EBAM) changes this situation because part geometry, material placement, and internal structure can be created in a single manufacturing step [2,3]. Recent foam-printing studies have shown that in situ foaming can reduce density and generate cellular morphology during deposition, but most of this work has focused on conventional thermoplastics, filament feedstocks, or foam formation as a lightweighting strategy only [2–4]. Nevertheless, the printing of shape-

memory polymer (SMP) foams remains much less developed. Specifically, a manufacturing route that combines foam formation, the printed architecture of complex geometry, and shape-memory recovery within a single connected process has not yet been clearly established [2,5].

SMPs are smart materials that can be programmed into a temporary shape and later recover their permanent shape when an external stimulus is applied [6,7]. In thermally responsive SMPs, heat is the most common trigger. The material is first heated above its glass transition temperature ($T_g$), deformed into a prescribed temporary shape, and cooled while the deformation is held under constraint, thereby fixing the temporary shape. Upon reheating, molecular mobility is restored and the stored deformation is released, allowing the material to return to its permanent shape [6,7]. In this context, 4D printing refers to additive manufacturing of structures that are printed in one configuration but are designed to change shape, property, or function over time after exposure to a prescribed stimulus [5–8]. Among SMPs, SMPUs are especially suitable for extrusion-based 4D printing because their segmented morphology provides the physical network and switching response required for recovery, while their thermoplastic character allows the same material to be melt processed, printed, and formulated with additives or foaming agents [5,9–11]. These features make SMPUs attractive for deployable structures, biomedical devices, soft robotic components, morphing systems, and lightweight actuating parts where the material must be manufactured, programmed, and recovered in a controlled manner [12–16].

Blowing agents are commonly used to introduce cellular structure into thermoplastics during melt polymer processing [2,17]. Physical blowing agents, such as carbon dioxide and nitrogen, can produce fine cellular structures, but they usually require gas delivery, pressure regulation, saturation, or specialized extrusion equipment, which limits their direct use in simple pellet-fed additive manufacturing systems [2,3]. Chemical blowing agents (CBAs) offer a more accessible route because they can be supplied as processable masterbatches and release gas through thermal decomposition within the polymer melt [17]. Common CBA systems include azodicarbonamide-based agents, bicarbonate/citric-acid systems, and hydrazide-based agents, with the released gases depending on the chemistry and formulation [17]. Recent foam material-extrusion studies have shown that in situ foaming can control porosity, density, and cellular morphology during printing [2–4]. These studies confirm that foam printing is feasible, but they leave an important process gap. The literature has not yet established how decomposition-driven gas release can be matched with the melt behaviour, deposition stability, cellular morphology, and thermally triggered recovery of a thermoplastic SMPU foam. Thus, foaming and recovery cannot be treated as separate outcomes, and the process must generate a stable cellular structure while preserving the thermal conditions needed for shape-memory actuation [5,9].

This is the gap addressed in the present study. Foam additive manufacturing has shown that cellular structures can be generated during 4D-printing, SMPU research has shown that thermoplastic polyurethanes can retain shape-memory function after extrusion-based processing, and recent work has begun to combine in situ foaming with 4D printing in PLA-based systems [2–5,9]. However, these advances have not yet been connected in a chemically foamed in-situ pellet-printed SMPU system. This connection is important because it could provide a filament-free and gas-cylinder-free route to lightweight printed structures that can also be programmed and recovered

[18]. The primary question is whether CBA decomposition, foam retention, deposited-road stability, cellular morphology, and thermally activated recovery can all be controlled within the same pellet-printing process. In this study, SMPU pellets are dry-blended with a 1 wt% TRACEL masterbatch, corresponding to 0.30 wt% active CBA, and processed using a filament-free EBAM system. The printed materials are evaluated through physical density measurement, cellular morphology, and shape-memory testing to establish an initial process-level understanding of CBA-assisted direct 4D foam printing of SMPU.

## 3. Materials and Experimental Methods

### *3.1 Materials and Feedstock Preparation*

A commercial SMPU used in this study was MM6520 from the DiAPLEX MM series supplied by SMP Technologies Inc., Japan. MM6520 is a thermoplastic polyurethane-based SMP supplied in pellet form and has a reported $T_g$ near 65 °C [5,9]. Thermogravimetric Analysis was performed to evaluate the thermal response of SMPU using a TA Instruments TGA Q50 at 10 °C/min under nitrogen. Foaming was introduced using TRACEL IM 3170 MS (TRAMACO GmbH, Germany), a polymer-bound activated azodicarbonamide CBA masterbatch. According to the supplier, TRACEL IM 3170 MS contains approximately 30 wt% active foaming agent, decomposes near 170 °C, and produces approximately 50 mL/g gas at 220 °C [19]. The reported evolved gases include nitrogen, carbon monoxide, carbon dioxide, and ammonia [19]. The masterbatch loading was fixed at 1 wt% of the total SMPU/TRACEL blend, corresponding to approximately 0.30 wt% active CBA. Before processing, MM 6520 pellets were dried at 80 °C for 48 h. This drying step was used to reduce moisture-related defects known to affect extrusion-based SMPU processing [20]. TRACEL IM 3170 MS was stored in a dry cabinet and dry-blended with the dried SMPU pellets immediately before processing.

### *3.2 Filament-Free 4D Printing System*

Filament-free 4D printing was performed using a Dyze Design Pulsar pellet extruder mounted on a 3DP 300 platform. In this system, the feedstock is introduced directly in pellet form, melted inside the heated barrel, and discharged through the nozzle. This processing route was selected to integrate pellet feeding, melt processing, CBA activation, and material deposition within a single manufacturing step. The pellet extruder contains three independently controlled heating zones. A schematic of the filament-free CBA-assisted 4D printing route is shown in Figure 1.

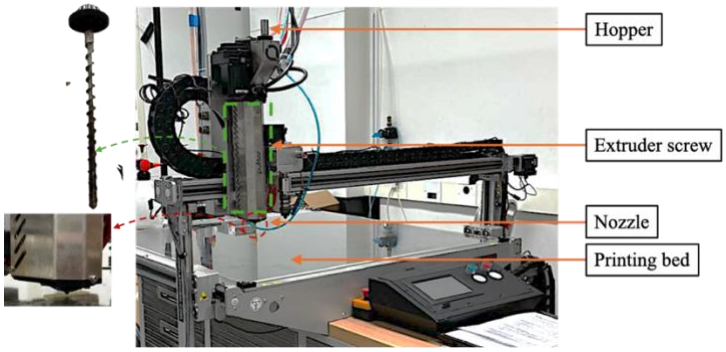


Figure 1 Schematic of the filament-free CBA-assisted 4D printing route

*3.3 Nozzle Screening and Density Measurement*

Nozzle screening was performed to evaluate the effect of nozzle restriction on the density and cellular morphology of solid (unfoamed) and foamed SMPU. Free extrudates were produced using 1 mm and 3 mm nozzles under the same barrel temperature profile of 190-200-210 °C from the feed zone to the nozzle zone and the same extrusion setting. The platform temperature was maintained at 60 °C. For density measurement, 300 mm long extrudates were collected after cooling to room temperature. The volume was calculated assuming cylindrical geometry, and the density was calculated using Eq. (1):

$$\rho = \frac{m}{V} \quad \text{Eq. (1)}$$

where $m$ is the specimen mass, and $V$ is the calculated volume of the free-extrudate.

The density-based expansion ratio (ER) was calculated as in Eq. (2).

$$ER = \frac{\rho_s}{\rho_f} \quad \text{Eq. (2)}$$

where $\rho_s$ is the density of the solid SMPU extrudate, and $\rho_f$ is the density of the foamed extrudate.

*3.4 Cellular Morphology*

The cellular morphology of the free-extrudates of solid and foamed SMPU was characterized using scanning electron microscopy (SEM). Cellular morphology was quantified from SEM micrographs using ImageJ2 version 2.16.0/1.54p [21]. The 1 mm and 3 mm extrudates had substantially different cross-sectional areas, therefore cellular morphology was compared using cell diameter, cell count, and area fraction rather than with cell density. Cell diameter was measured directly from the visible cell openings, and cell count was obtained from the same selected region. The cell area fraction ($\Phi_A$) was calculated from the total measured cell area relative to the selected cross-sectional area of the free-extrudate, as shown in Eq. (3) [22,23].

$$\Phi_A = \frac{\sum A_i}{A_{ROI}} \quad \text{Eq. (3)}$$

where $A_i$ is the area of an individual cell, and $A_{ROI}$ is the cross-sectional region of interest.

*3.5 Single-Road Specimen Fabrication*

The shape-memory specimens were 4D-printed as single-road deposited tracks using the same barrel temperature profile of 190-200-210 °C for solid and foamed SMPU. The deposition path was sliced in Simplify3D v4.1.2 using the parameters listed in Table 1.

Table 1 Deposition parameters used to fabricate single-road specimens for free-recovery testing.

| **Parameter** | **Value** |
|---|---|
| Extrusion width | 4.8 mm |

| | |
|---|---|
| Extrusion multiplier | 0.5 |
| Layer height | 5.0 mm |
| Printing speed | 300 mm/min |
| Bed setpoint | 60 °C |

*3.6 Shape-Memory Free-recovery Testing*

Shape-memory recovery tests were performed using 80 mm long single-road deposited tracks. Both solid and foamed SMPU specimens were tested in a three-point bending configuration [24]. In this study, a 60 mm gauge span was used, leaving 10 mm on each side of the specimen. Temporary-shape programming was performed at 80 °C. The specimen was deformed by the upper fixture, held under constraint during cooling to room temperature, and then unloaded before recovery. Free recovery was induced by heating the programmed specimens to 80 °C at a heating rate of 5 °C/min. For optical tracking, a Basler acA3800-10gm camera was used to track the specimen surface, which was coated with a thin black spray-paint layer and then covered with a straight line white speckle pattern. The shape recovery ratio (SRR) was calculated with Eq. (4) [5,9].

$$SRR = \left(\frac{S_i - S_n}{S_i - S_0}\right) \times 100 \qquad \text{Eq. (4)}$$

where $S_i$ is the initial deflection at the beginning of recovery, $S_0$ is the initial undeformed midspan position prior to programming, and $S_n$ is the midspan deflection at time n.

## 4. Results and Discussion

*4.1 Density and Expansion Behaviour*

The density measurements show that retained foaming was strongly dependent on nozzle size. Table 2 summarizes the density, diameter, expansion ratio, and density reduction of solid SMPU and 1 wt% TRACEL/SMPU extrudates produced using 1 mm and 3 mm nozzles. The solid SMPU extrudates had similar densities for both nozzle conditions, with 1230.2 ± 53.7 kg m$^{-3}$ for the 1 mm nozzle and 1242.1 ± 15.4 kg m$^{-3}$ for the 3 mm nozzle. This provides a consistent reference for evaluating the effect of TRACEL addition. The 1 mm TRACEL/SMPU extrudate showed limited retained expansion. Its density was 1255.8 ± 47.8 kg m$^{-3}$, corresponding to an expansion ratio of 0.97 and a density reduction of -2.9% relative to the solid SMPU. In contrast, the 3 mm TRACEL/SMPU extrudate showed a clear foaming response, with density decreasing from 1242.1 ± 15.4 kg m$^{-3}$ for solid SMPU to 893.4 ± 79.3 kg m$^{-3}$. This corresponds to an expansion ratio of 1.39 and a density reduction of 28.1%, confirming that the selected filament-free processing route can retain CBA-generated gas as internal porosity under suitable nozzle conditions.

Table 2 Density and expansion response of solid SMPU and 1 wt% TRACEL/SMPU extrudates produced using 1 mm and 3 mm nozzles.

| **Material** | **Nozzle condition** | **Density (kg/m³)** | **Diameter (mm)** | **Expansion ratio** | **Density reduction** |
|---|---|---|---|---|---|

| | | | | | |
|---|---|---|---|---|---|
| SMPU | 1 mm | 1230.2 ± 53.7 | 2.317 ± 0.04 | - | - |
| 1 wt% TRACEL/SMPU | | 1255.8 ± 47.8 | 1.973 ± 0.18 | 0.97 | -2.9% |
| SMPU | 3 mm | 1242.1 ± 15.4 | 5.326 ± 0.04 | - | - |
| 1 wt% TRACEL/SMPU | | 893.4 ± 79.3 | 5.679 ± 0.19 | 1.39 | 28.1% |

The comparison shows that CBA-generated gas reduced the extrudate density only when the nozzle condition allowed gas expansion and retention before cooling. In chemical foam extrusion and in-situ foam printing, retained expansion is governed by the balance between blowing-agent decomposition, melt pressure, pressure release at the nozzle exit, melt strength, cooling rate, and geometric confinement [2–4,17]. The 3 mm nozzle provided more favourable conditions for gas expansion after pressure release, leading to the lower measured density and higher expansion ratio.

*4.2 Cellular Morphology*

The SEM observations confirm that CBA addition generated cellular structure during filament-free processing. As shown in Figure 2, solid SMPU extrudates exhibited dense cross-sections, whereas the 1 wt% TRACEL/SMPU extrudates contained visible cells. The degree of cell development, however, depended strongly on nozzle size.

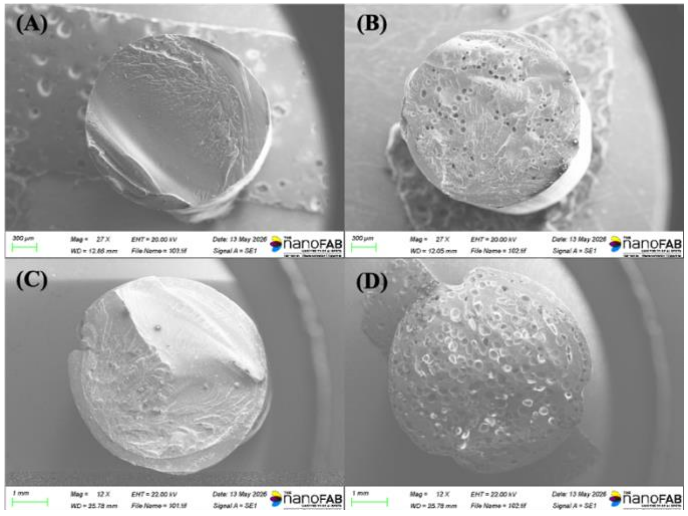


Figure 2 Representative SEM micrographs: 1 mm Nozzle for (A) Solid SMPU and (B) 1 wt% TRACEL/SMPU, and 3 mm Nozzle for (C) Solid SMPU and (D) 1 wt% TRACEL/SMPU.

The 1 mm 1 wt% TRACEL/SMPU contained relatively small cells, with an average cell diameter of 59.1 ± 7.0 µm and a cell area fraction of 5.4 ± 1.4%, as shown in Table 3. This limited cellular area is consistent with the density results in Table 2, where the 1 mm TRACEL/SMPU extrudate showed limited retained expansion. In contrast, the 3 mm nozzle produced a more developed cellular structure for 1 wt% TRACEL/SMPU, with a larger average cell diameter of 158.2 ± 13.3 µm, higher cell count, and higher cell area fraction of 16.7 ± 4.8%. These morphology results support the measured density reduction of the 3 mm foamed extrudate, indicating that a greater portion of the CBA-generated gas was retained within the extrudate cross-section.

Table 3 Cellular morphology of 1 wt% TRACEL/SMPU extrudates using 1 mm and 3 mm nozzles.

| Nozzle condition | Cell diameter (µm) | Cell count | Cell area fraction |
|---|---|---|---|
| 1 mm | 59.1 ± 7.0 | 57.7 ± 23.1 | 5.4 ± 1.4% |
| 3 mm | 158.2 ± 13.3 | 191.7 ± 29.6 | 16.7 ± 4.8% |

This nozzle-dependent morphology is consistent with CBA-assisted foam extrusion and in situ foam printing, where cell growth is governed by the coupling between gas generation, melt pressure, pressure release at the nozzle exit, melt strength, residence time, and cooling after extrusion [2–4,17]. The smaller nozzle likely increased geometric confinement during gas evolution, producing a finer cellular structure with limited cross-sectional expansion. The 3 mm nozzle provided more favourable conditions for bubble growth after pressure release, resulting in larger cells, a greater cell area fraction, and a lower measured density.

*4.3 Shape-Memory Free Recovery*

Shape-memory free-recovery tests were performed on single-road specimens fabricated with the 3 mm nozzle, which was selected as it produced measurable density reduction and a developed cellular structure. Figure 3 shows a representative free-recovery sequence for a specimen programmed in a three-point bending configuration. Both solid SMPU and 1 wt% TRACEL/SMPU recovered their original configuration after heating to 80 °C, confirming that the thermally activated recovery response was preserved after filament-free foaming.

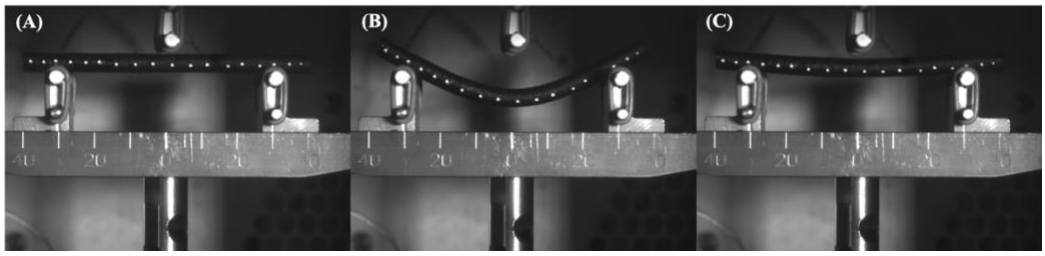


Figure 3 Representative shape-memory free-recovery of single-road deposited SMPU specimens: (A) original shape, (B) programmed temporary shape, and (C) recovered shape.

The solid SMPU specimens showed a SRR of 97.5 ± 2.6%, indicating nearly complete recovery under the selected programming and recovery conditions. The 1 wt% TRACEL/SMPU specimens showed a lower recovery ratio of 84.9 ± 2.0%, while still retaining substantial shape-memory functionality. In thermally activated SMPs, the temporary shape is fixed by cooling the deformed polymer below its $T_g$, and recovery occurs when reheating restores chain mobility and releases the stored deformation [6,7]. In the foamed specimens, the cells introduce local discontinuities in the printed road and concentrate deformation in the surrounding cell walls during bending. After unloading and reheating, these regions can retain more residual deformation than the solid material, particularly under free-recovery conditions where recovery occurs without an applied external force. Similar behaviour has been reported for foamed thermoplastic polyurethane and SMP foam systems, where recovery is influenced by cell morphology, foam density, stiffness, and

recovery stress [5,9]. Although foaming reduced the recovery ratio compared with solid SMPU, the 1 wt% TRACEL/SMPU specimens still recovered 84.9 ± 2.0% after achieving a 28.1% density reduction with the 3 mm nozzle. This result shows that filament-free CBA-assisted processing can introduce internal porosity and reduce SMPU density while retaining a thermally triggered shape-memory response.

## 5. Conclusion

This study establishes a filament-free route for manufacturing lightweight SMPU foams with preserved thermally activated shape-memory functionality. By combining pellet-based extrusion with a CBA masterbatch, the work connects foam formation, deposited-road fabrication, density reduction, cellular morphology, and shape-recovery response within a single processing route. This connection is central to developing foam 4D printing, where the printed material must provide both structural lightweighting and programmable shape change. The nozzle-screening results showed that the processing condition governed the retention of CBA-generated gas. The 1 mm nozzle produced visible cellular structure but limited macroscopic expansion, giving an expansion ratio of 0.97. The 3 mm nozzle provided a more favourable condition for gas growth and retention, reducing the density from 1242.1 ± 15.4 kg $m^{-3}$ for solid SMPU to 893.4 ± 79.3 kg $m^{-3}$ for 1 wt% TRACEL/SMPU. This corresponds to an expansion ratio of 1.39 and a density reduction of 28.1%. SEM analysis confirmed that this density reduction was associated with a more developed cellular morphology, including larger cells, higher cell count, and greater cell area fraction. The shape-memory results confirmed that the functional response of SMPU was preserved after foaming. Solid SMPU recovered 97.5 ± 2.6% after programming, while 1 wt% TRACEL/SMPU recovered 84.9 ± 2.0% after achieving the 28.1% density reduction. The reduction in SRR reflects the influence of cellular morphology on local deformation, while the retained recovery demonstrates that the SMPU network remained thermally active after CBA-assisted processing.

Overall, the study identifies nozzle-controlled foam retention as the key process link between lightweighting and shape-memory performance. The results show that filament-free CBA-assisted processing can produce SMPU foams with meaningful density reduction while maintaining thermally triggered recovery. This provides a process-level foundation for adaptive lightweight foam structures produced by 4D printing, with potential relevance to deployable systems, morphing components, and soft robotic architectures.

## 6. References

[1] L.J. Gibson, M.F. Ashby, Cellular solids: Structure and properties, second edition, Cellular Solids: Structure and Properties, Second Edition (2014) 1–510. https://doi.org/10.1017/CBO9781139878326.

[2] M. Nofar, J. Utz, N. Geis, V. Altstädt, H. Ruckdäschel, Foam 3D Printing of Thermoplastics: A Symbiosis of Additive Manufacturing and Foaming Technology, Advanced Science 9 (2022) 2105701. https://doi.org/https://doi.org/10.1002/advs.202105701.

[3] K. Kalia, B. Francoeur, A. Amirkhizi, A. Ameli, In Situ Foam 3D Printing of Microcellular Structures Using Material Extrusion Additive Manufacturing, ACS Appl. Mater. Interfaces 14 (2022) 22454–22465. https://doi.org/10.1021/ACSAMI.2C03014.

[4] K. Kalia, A. Ameli, Understanding the process-microstructure-property relationships in material extrusion additive manufacturing of polylactic acid microcellular foams, Addit. Manuf. 72 (2023) 103636. https://doi.org/10.1016/J.ADDMA.2023.103636.

[5] D. Kashyap, P. Kishore Kumar, S. Kanagaraj, 4D printed porous radiopaque shape memory polyurethane for endovascular embolization, Addit. Manuf. 24 (2018) 687–695. https://doi.org/10.1016/J.ADDMA.2018.04.009.

[6] Shape-Memory Polymers - Lendlein - 2002 - Angewandte Chemie International Edition - Wiley Online Library, (n.d.). https://onlinelibrary.wiley.com/doi/10.1002/1521-3773(20020617)41:12%3C2034::AID-ANIE2034%3E3.0.CO;2-M (accessed May 28, 2026).

[7] M. Behl, A. Lendlein, Shape-memory polymers, Materials Today 10 (2007) 20–28. https://doi.org/10.1016/S1369-7021(07)70047-0.

[8] I.T. Garces, C. Ayranci, Advances in additive manufacturing of shape memory polymer composites, Rapid Prototyp. J. 27 (2021) 379–398. https://doi.org/10.1108/RPJ-07-2020-0174.

[9] I. Tatiana, G. Arguello, Shape Memory Polymers and Their Composites: Towards Field Applications via Production, Characterization and Modelling, (2021). https://doi.org/10.7939/R3-CBD0-V604.

[10] J. Raasch, M. Ivey, D. Aldrich, D.S. Nobes, C. Ayranci, Characterization of polyurethane shape memory polymer processed by material extrusion additive manufacturing, Addit. Manuf. 8 (2015) 132–141. https://doi.org/10.1016/J.ADDMA.2015.09.004.

[11] W.A. Pancho Ramirez, R. Ahmad, C. Ayranci, Influence of 4D printing parameters on the stored pre-strain of flat structures fabricated with polyurethane-based shape memory polymer (SMPU), Progress in Additive Manufacturing 2025 10:9 10 (2025) 6673–6690. https://doi.org/10.1007/S40964-025-00999-5.

[12] J. Villacres, D. Nobes, C. Ayranci, Additive manufacturing of shape memory polymers: effects of print orientation and infill percentage on mechanical properties, Rapid Prototyp. J. 24 (2018) 744–751. https://doi.org/10.1108/RPJ-03-2017-0043.

[13] I.T. Garces, C. Ayranci, Active control of 4D prints: Towards 4D printed reliable actuators and sensors, Sens. Actuators A Phys. 301 (2020) 111717. https://doi.org/10.1016/J.SNA.2019.111717.

[14] I.T. Garces, S. Aslanzadeh, Y. Boluk, C. Ayranci, Cellulose nanocrystals (CNC) reinforced shape memory polyurethane ribbons for future biomedical applications and design, Journal

of Thermoplastic Composite Materials 33 (2020) 377–392. https://doi.org/10.1177/0892705718806334.

[15] I.T. Garces, C. Ayranci, A view into additive manufactured electro-active reinforced smart composite structures, Manuf. Lett. 16 (2018) 1–5. https://doi.org/10.1016/J.MFGLET.2018.02.008.

[16] Y. Chen, I.T. Garces, T. Tang, C. Ayranci, Cellulose nanocrystals reinforced shape memory polymer cardiovascular stent, Rapid Prototyp. J. 27 (2021) 37–44. https://doi.org/10.1108/RPJ-01-2020-0019.

[17] R.M. Aseeva, K. Ashida, J.K. Backus, T. Baumann, R. Broos, L. Domeier, C. V Gupta, J.R. Harper, R. Herrington, P.T. Kelly, D. Klempner, P. Knaub, R.F. Mausser, W. Nicholson, C.B. Park, C.P. Park, J.H. Saunders, V. Sendijarevic, F.A. Shutov, K.W. Suh, D. Visco, F.X. Hanser, Handbook of Polymeric Foams and Foam Technology 2nd Edition Edited by Daniel Klempner and Vahid Sendijarevic With contributions by, (n.d.).

[18] M.V. Paez Estrella, I. Garces, C. Ayranci, Direct 4D printing: pellet extrusion of shape memory polymer composites with large-scale additive manufacturing machine, Rapid Prototyp. J. 32 (2026) 1066–1078. https://doi.org/10.1108/RPJ-07-2025-0313.

[19] Chemical blowing agents for polyolefin extrusion | TRAMACO, (n.d.). https://www.tramaco.de/en/products/blowing-agents-and-additives/chemical-blowing-agents-for-polyolefin-extrusion/ (accessed May 28, 2026).

[20] I.T. Garces, S. Aslanzadeh, Y. Boluk, C. Ayranci, Effect of Moisture on Shape Memory Polyurethane Polymers for Extrusion-Based Additive Manufacturing, Materials 2019, Vol. 12, Page 244 12 (2019) 244. https://doi.org/10.3390/MA12020244.

[21] C.T. Rueden, J. Schindelin, M.C. Hiner, B.E. DeZonia, A.E. Walter, E.T. Arena, K.W. Eliceiri, ImageJ2: ImageJ for the next generation of scientific image data, BMC Bioinformatics 2017 18:1 18 (2017) 529-. https://doi.org/10.1186/S12859-017-1934-Z.

[22] Practice for Determining the Inclusion or Second-Phase Constituent Content of Metals by Automatic Image Analysis, (2016). https://doi.org/10.1520/E1245-03R16.

[23] J.C. Russ, R.T. Dehoff, Practical Stereology, Practical Stereology (2000). https://doi.org/10.1007/978-1-4615-1233-2.

[24] J. Villacres, D. Nobes, C. Ayranci, Additive manufacturing of shape memory polymers: effects of print orientation and infill percentage on shape memory recovery properties, Rapid Prototyp. J. 26 (2020) 1593–1602. https://doi.org/10.1108/RPJ-09-2019-0239.